Available online at www.sciencedirect.com

SciVerse ScienceDirect

Ceramics International 38 (2012) 3595–3606

CERAMICS INTERNATIONAL

www.elsevier.com/locate/ceramint

Thermal shock behavior of 8YSZ and double-ceramic-layer $La_2Zr_2O_7$/8YSZ thermal barrier coatings fabricated by atmospheric plasma spraying

L. Wang [a,b,*], Y. Wang [a,**], X.G. Sun [a,c], J.Q. He [a], Z.Y. Pan [a], C.H. Wang [a,d]

[a] Laboratory of Nano Surface Engineering, Department of Materials Science, School of Materials Science and Engineering, Harbin Institute of Technology, Harbin 150001, PR China

[b] State Key Laboratory of High Performance Ceramics and Superfine Microstructure, Shanghai Institute of Ceramics, Chinese Academy of Sciences, Shanghai 200050, PR China

[c] Department of Chemical and Materials Engineering, University of Alberta, Edmonton, AB, Canada T6G 2V4

[d] School of Materials Science and Engineering, Qiqihar University, Qiqihar 161006, PR China

Received 27 November 2011; received in revised form 29 December 2011; accepted 29 December 2011
Available online 5 January 2012

Abstract

The single-ceramic-layer (SCL) 8YSZ (conventional and nanostructured 8YSZ) and double-ceramic-layer (DCL) $La_2Zr_2O_7$ (LZ)/8YSZ thermal barrier coatings (TBCs) were fabricated by plasma spraying on nickel-based superalloy substrates with NiCrAlY as the bond coat. The thermal shock behavior of the three as-sprayed TBCs at 1000 °C and 1200 °C was investigated. The results indicate that the thermal cycling lifetime of LZ/8YSZ TBCs is longer than that of SCL 8YSZ TBCs due to the fact that the DCL LZ/8YSZ TBCs further enhance the thermal insulation effect, improve the sintering resistance ability and relieve the thermal mismatch between the ceramic layer and the metallic layer at high temperature. The nanostructured 8YSZ has higher thermal shock resistance ability than that of the conventional 8YSZ TBC which is attributed to the lower tensile stress in plane and higher fracture toughness of the nanostructured 8YSZ layer. The pre-existed cracks in the surface propagate toward the interface vertically under the thermal activation. The nucleation and growth of the horizontal crack along the interface eventually lead to the failure of the coating. The crack propagation modes have been established, and the failure patterns of the three as-sprayed coatings during thermal shock have been discussed in detail.

Keywords: C. Thermal shock resistance; Atmospheric plasma spraying; Thermal barrier coatings

1. Introduction

In aerospace industry, achieving higher efficiency for gas turbines and aircraft engines has always been an important research area. Higher efficiency requires the gas turbines to operate at higher temperatures. However, such high heat input weakens the structure of the gas turbine. Therefore, ceramic thermal barrier coatings (TBCs) are widely used as insulation materials protecting the underlying metallic structure of a gas turbine blade [1–5]. In the foreseeable future, advanced engines may be expected to rely even more heavily on these coatings.

The TBCs are often composed of several layers. The typical TBC is composed of double layers including the bond coat and top coat. The bond coat is MCrAlY (where M = Ni and/or Co) which can relieve the thermal mismatch between the ceramic layer and the substrate. The top-coat is often composed of 6–8 wt.% yttria stabilized zirconia (YSZ). The yttria often plays an important role in impeding the occurrence of the phase transformation from t-ZrO_2 to m-ZrO_2, because this phase transformation can produce 3–5% volume expansion [6,7]. Cracking and failure is inevitable in this process. Generally, there are two common ways to fabricate the TBC, i.e. atmospheric plasma spraying (APS) and electrical beam-physical vapor deposition (EB-PVD) [8–11]. The APS coating usually shows a laminar structure, in which pores and cracks are inevitable due to the internal thermal stress in the process of

* Corresponding author at: Laboratory of Nano Surface Engineering, Department of Materials Science, School of Materials Science and Engineering, Harbin Institute of Technology, Harbin 150001, PR China.
Tel.: +86 451 8640 2752; fax: +86 451 8641 3922.
** Corresponding author. Tel.: +86 451 8640 2752; fax: +86 451 8641 3922.
E-mail addresses: glacier_siccas@126.com, glacier_hit@126.com (L. Wang), wangyou@hit.edu.cn (Y. Wang).

0272-8842/$36.00.
doi:10.1016/j.ceramint.2011.12.076

thermal spraying. By contrast, the coating fabricated by EB-PVD exhibits columnar grain structure. And large amounts of sub-grains are distributed between the adjacent columnar grains. Generally, the APS coating has low thermal conductivity which is attributed to the existence of large amounts of defects. The EB-PVD coating often has high strain tolerance and high thermal shock resistance ability. Despite unique advantages for the two kinds of TBCs, cracks and interfacial debonding of the ceramics coatings are the undesirable problems associated with TBCs during the long-term high temperature service [12–17]. This is primarily due to the fact that ceramics and metal have very different properties. The high brittleness combined with low thermal expansion and thermal conductivity renders TBCs highly susceptible to the generation of thermal stresses with high magnitude.

Zirconate-based TBCs are expected to be the candidate materials for the future application in aircraft, turbine and other high temperature components due to its low thermal conductivity, high stability and high sintering resistance ability at high temperature [18–25]. $La_2Zr_2O_7$ (LZ) is one of the candidate materials that can be used for TBCs. Many literatures have reported the thermal physical properties of zirconate-based bulk ceramic materials, but very little investigation was focused on the zirconate-based TBCs. Some literatures have reported the thermal shock behavior and hot corrosion behavior of zirconate-based TBCs fabricated by EB-PVD [26–30]. Little investigation was focused on the thermal shock behavior of the double-ceramic-layer (DCL) TBCs fabricated by (APS). In this paper, the DCL LZ/8YSZ TBCs and single-ceramic-layer (SCL) 8YSZ TBCs were fabricated by APS and their thermal shock behavior was investigated systematically.

2. Experimental procedures

2.1. Preparation of feedstocks used for thermal spraying

The nanostructured agglomerated feedstocks which can be used for plasma spraying were obtained by the spray drying granulation method. The critical steps including: ball milling, spray drying, calcination and plasma treatment. The basic preparation procedure of the sprayable LZ feedstock can be described as follows: slurry for spray-drying which was composed of nano-sized La_2O_3 and ZrO_2 ceramic powders, polyvinyl alcohol (PVA) and deionized water was ball milled for longer than 24 h. Secondly, the slurry was sprayed into small droplets with the help of a LPG-10 high-speed centrifugal spray dryer (Qiangli Drying Equipment Co., Ltd., Changzhou, China) equipped with a pneumatic nozzle (external mixing) and a high-speed rotary atomizer. Thirdly, the spray dried powder after spray drying was calcined at 1350 °C for 2 h according to the thermal behavior of the spray dried powder after the first time spray drying. Fourthly, the as spray dried powder was further ball milled. In the last step, the slurry was spray dried and the sprayable LZ feedstock can be obtained. The detailed preparation procedure of LZ feedstock and the corresponding technological parameters can be seen in our previous work [31].

2.2. Preparation of coatings

All coatings were fabricated by plasma spraying. Before spraying, the superalloy (GH4169) substrates were immersed in the ethanol for ultrasonic cleaning with the dwell time 15 min. After taking out the substrates, the substrates were then degreased and grit-blasted with 24 mesh brown corundum in order to increase the bonding strength. The feedstock was dried in an oven at 120 °C for 2 h, and the powder with the size below 200 mesh was collected as the thermal sprayed feedstock. Then NiCrAlY, YSZ and LZ coating were deposited onto the superalloy substrates in turn to fabricate the DCL LZ/8YSZ TBCs. The SCL 8YSZ TBCs were prepared without depositing LZ coating. All the feedstocks were thermally sprayed using an Ar/H2 APS torch (9MB plasma gun, GH nozzle, Sulzer Metco, Westbury, NY, USA). The feedstocks which were used to deposit the coatings were given externally. The thermal spray parameters are displayed in Table 1. The thickness of the produced TBCs was 300 μm (including the bond coat and the ceramic coat), the thickness of the bond coat of all the coatings is about 100 μm. As for the DCL LZ/8YSZ, the thicknesses of the 8YSZ layer and the LZ layer are 240 μm and 60 μm, respectively.

2.3. Thermal shock resistance testing

Thermal shock resistance test was performed by heating and water quenching method. The coatings were deposited onto the cylinder like superalloy substrates with the size Ø20 mm × 6 mm. The samples were put into the high temperature muffle furnace and were heated to 1000 °C (1200 °C) with the dwell time 5 min, then they were thrown into the water with the temperature 20 °C quickly. When the coating samples were cooled to the ambient temperature, they were taken out, dried and put into the high temperature muffle furnace again, repeat the same process. The thermal cycle number when nearly 20% coating surface was destroyed (cracking and peeling is visible to the naked eye) was recorded as the thermal cycling lifetime of the as-sprayed coating. The dynamic macro-images of the destroyed coating samples were captured by a digital camera timely. The composition and microstructure of the fracture surface was examined by X-ray diffraction (XRD, D/max2400, RIGAKU, Japan) and Scanning

Table 1
Parameters used in the plasma spraying.

Parameter	NiCoCrAlY	ZrO_2–8%Y_2O_3	$La_2Zr_2O_7$
Current (A)	530	570	650
Voltage (V)	53	55	60
Flow rate of primary gas (SCFH[a])	120	100	100
Feedstock giving rate (g/min)	5.0	6.8	6.3
Spray distance (mm)	110	80	100
Spray angle (°)	90	90	90
Spray velocity (mm/s)	30	30	390

[a] SCFH = 0.472 L min^{-1}.

Electric Microscope (SEM, S-570, Hitachi, Tokyo, Japan) equipped with Energy Dispersion Spectrum (EDS).

3. Results and discussion

3.1. Microstructure of the feedstock and corresponding coating

Fig. 1 shows the morphology of the three kinds of feedstocks. From Fig. 1(a) it is clear that the conventional feedstock exhibits polyhedral, irregular and angular shape with different sizes ranging from 10 μm to 40 μm which may due to its obtaining from sintering and crushing in the actual process, and this will affect its flowability and decrease the deposition efficiency more or less in the plasma spraying process. The nanostructured feedstock is composed of spherical/equiaxed shape of nanostructured agglomerates with the size of 10–50 μm. It can be designated as sphere package structure (Fig. 1(b)). The LZ feedstock has similar microstructure, but the size distribution is in the range of 15–35 μm (Fig. 1(c)).

Fig. 2 displays the XRD patterns of the three feedstocks and corresponding coatings. The conventional powder is mainly composed of $Y_{0.15}Zr_{0.85}O_{1.93}$, m-$ZrO_2$ and c-ZrO_2 (Fig. 2(a)), and the corresponding coating is mainly composed of $Y_{0.15}Zr_{0.85}O_{1.93}$, c-$ZrO_2$ after the plasma spraying process (Fig. 2(b)). The nanostructured 8YSZ feedstock is mainly composed of t phase (Fig. 2(c)), the corresponding coating is predicted to be composed of t′ phase after the plasma spraying

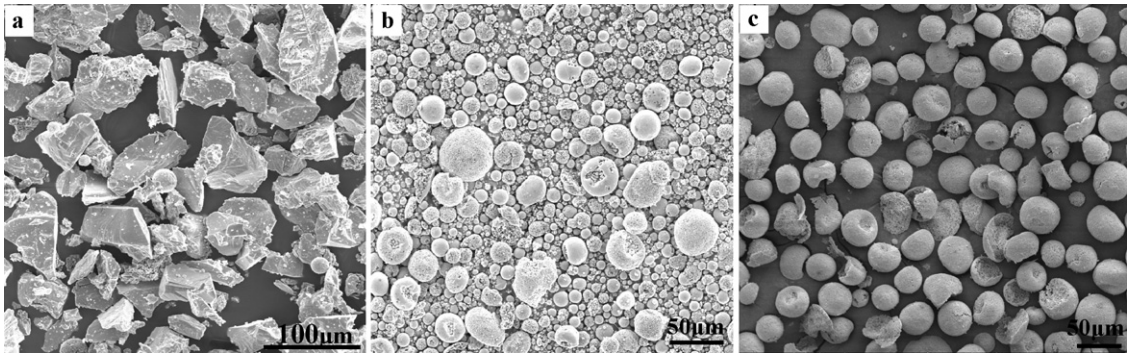

Fig. 1. Surface morphology of thermal sprayed feedstock: (a) conventional 8YSZ, (b) nanostructured 8YSZ agglomerates, and (c) nanostructured LZ feedstock.

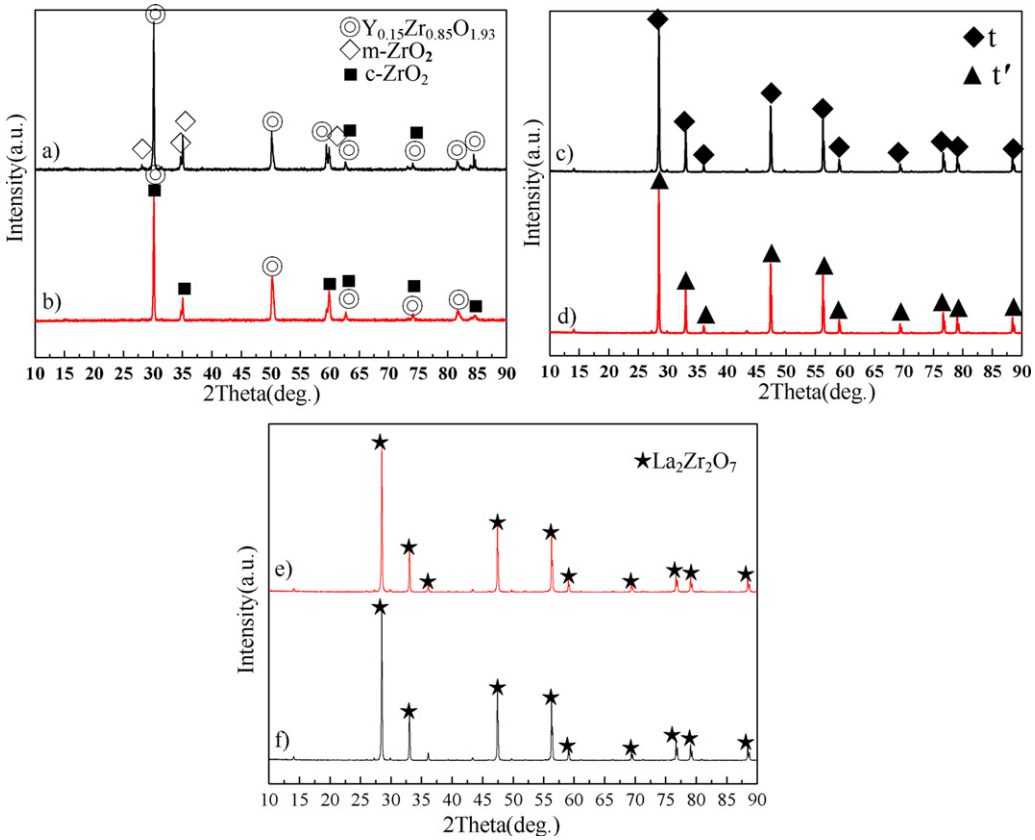

Fig. 2. XRD patterns of thermal sprayed feedstocks and corresponding coatings: (a) conventional 8YSZ feedstock and (c) conventional 8YSZ coating, (e) nanostructured 8YSZ coating, (b) nanostructured 8YSZ agglomerated feedstock, (d) nanostructured LZ coating, and (f) nanostructured LZ feedstock.

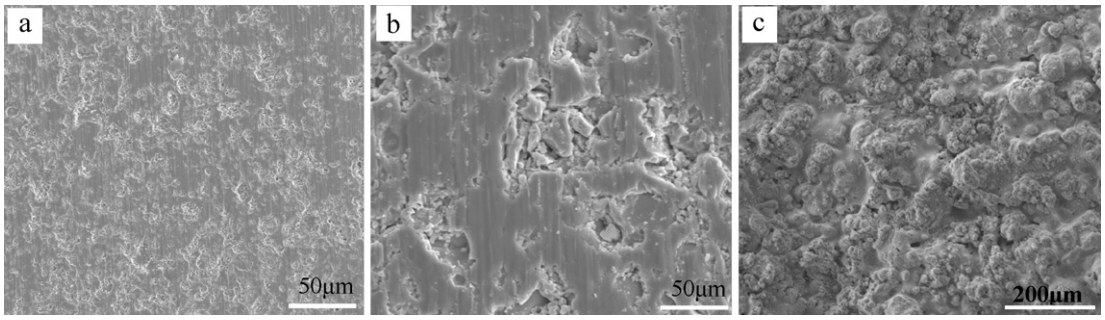

Fig. 3. Surface morphology of (a) conventional 8YSZ TBCs, (b) nanostructured 8YSZ TBCs, and (c) LZ/8YSZ TBCs.

process (Fig. 2(d)). This tetragonal zirconia phase which was observed in the as-sprayed coating is mainly composed of so-called non-transformable phase t′. It has lower c and c/a compared with the t phase (where a, c denote the lattice parameters) [32]. The free yttria phase is not observed in the XRD pattern of the nanostructured as-sprayed zirconia coatings. It is usually recognized that the t′ phase resulted from the high temperature cubic phase by a diffusionless transformation at high quenching rate of 10^6 K/s. The t phase is normal tetragonal phase. And the content of the Y_2O_3 in the t phase is lower compared with t′ phase. While the LZ agglomerated feedstock formed single phase in the process of solid state reaction and spray drying granulation, and the LZ phase keep stable during the plasma spraying which indicate that the phase structure of LZ coating is very stable (Fig. 2(e) and (f)).

Fig. 3 displays the surface morphology of the three as-sprayed coatings. The surface of the conventional TBCs is uneven. The microstructure is not uniform and compact. A certain quantity of pores and micro-cracks can be observed (Fig. 3(a)). This surface morphology is closely correlated with the formation mechanism of the coating. When compared with the conventional TBCs (prepared by conventional micron-sized powders ZrO_2–8 wt.%Y_2O_3), the surface of the nanostructured 8YSZ TBCs is much smoother. The microstructure is more compact and less porous. The surface cracks are relatively finer due to the increasing toughness of the nanostructured coating. Fig. 3(c) shows the surface morphology of the plasma sprayed LZ/8YSZ coating. It can be noticed that the surface of LZ layer is not smooth. There are some half-melted fluffy particles and many different sizes of pores, voids and cracks due to the insufficient overlapping among the adjacent molten drops in the plasma spraying process, while the presence of cracks is caused by the internal residual stress after plasma spraying.

3.2. Thermal cycling lifetime and macro fracture image

Fig. 4 shows the thermal cycling lifetime of the three kinds of coatings at 1000 °C and 1200 °C. It can be seen that the DCL LZ/8YSZ TBCs has the longest thermal cycling lifetime at different temperatures, the conventional SCL 8YSZ TBCs has the shortest thermal cycling lifetime. With the temperature increasing, the thermal cycling lifetime of all the three coatings decrease due to higher temperature gradient and thermal stress gradient in the coating system. Especially, when the temperature increases to 1200 °C, the thermal cycling lifetime of the DCL LZ/8YSZ TBCs is twice more than that of the nanostructured SCL 8YSZ TBCs. The large thermal stress will promote the failure of the coatings. Generally speaking, failure in thermal barrier coatings is associated with the build-up of stress mainly due to oxide scale growth and thermal expansion mismatch. When the coating specimen was taken out from the high temperature furnace and quickly quenched in water in the process of thermal cycling, very large stress developed in the coating due to the difference of thermal expansion coefficients between the ceramic layer and the metallic substrate, which can be given by the following expression:

$$\sigma_c = \frac{E_c \Delta\alpha \Delta T}{1 - \nu_c^2} \tag{1}$$

where σ_c is the developed stress in the coating. E_c and ν_c are Young's modulus and Poisson ratio of the ceramic coating, respectively. $\Delta\alpha$ is the difference in coefficients of thermal expansion between the ceramic coating and the metallic substrate, and ΔT is the change in temperatures. It can be seen from Eq. (1), as the thermal shock stress has a linear relationship with the temperature difference ΔT, the coating at 1000 °C has a longer thermal cycling lifetime compared with the case at 1200 °C due to the decrease of the developed stress in the coating.

Fig. 5 displays the macro-image of coatings after thermal cycle testing. It can be seen that when the thermal cycling temperature is 1000 °C, the convnetional and nanostructured

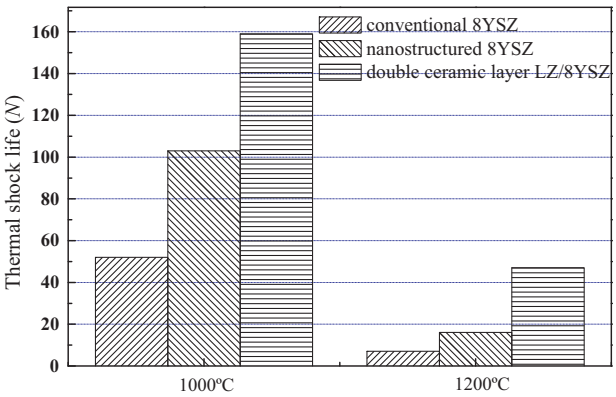

Fig. 4. Thermal cycling lifetime of different coatings at different thermal shock temperature.

SCL 8YSZ TBCs began to peel off from the brim of the coating after 11 and 17 times, respectively. And the crack propagates to the center of the coating specimen. The thermal cycling lifetimes of conventional SCL 8YSZ and nanostructured SCL 8YSZ TBCS are 53 and 104 times, respectively. As for the DCL LZ/8YSZ TBCs, after 46 thermal cycles, there is no obvious change for this coating, and the thermal cycling lifetime of this coating is 158 times. Fig. 6 shows the macro-image of coatings after thermal cycle testing at 1200 °C. The convnetional and nanostructured SCL 8YSZ TBCs began to peel off from the brim of the coating after 3 and 9 times, respectively. And the crack propagates to the center of the coating specimen. The thermal cycling lifetimes of conventional SCL 8YSZ and nanostructured SCL 8YSZ TBCS are 7 and 18 times, respectively. As for the DCL LZ/8YSZ TBCs, after 26 themal cycles, there is also no obvious change for this coating, and the thermal cycling lifetime of this coating reach to 43 times. When combine Fig. 5 with Fig. 6, it can be noticed that the DCL has the best thermal shock resistance at high temperature. Why this kind of coating has the best thermal shock resistance ability at high temperature will be further investigated in the following aspects of this paper. To sum up, the spallation of the coatings initiated firstly in the relatively high stress areas associated with the geometry of the specimens, such as nearby the defects and at the extreme edges. After the specimen failed, the central coating of the top coat was still adhered to the substrate perfectly. The failure modes and mechanism of the three as-sprayed coatings at different temperatures will be further analyzed and discussed in detail in the following section of this paper.

3.3. Phase composition after thermal shock failure at different temperatures

Fig. 7 displays the XRD patterns of the three coatings after thermal shock failure. As for the conventional SCL 8YSZ TBCs, when the temperature is 1000 °C, the phase composition of the fracture surface is mainly t-ZrO_2 and $Zr_{0.92}Y_{0.08}O_{1.96}$. When the temperature increase to 1200 °C, the c-ZrO_2, $Y_{0.15}Zr_{0.85}O_{1.93}$ and some other phases which came from the bond coat can be detected. It can be concluded that the failure position after thermal cycling for the conventional SCL 8YSZ TBCs is at the inner of the upper 8YSZ ceramic layer. While at 1200 °C, the failure position may be at the ceramic-layer/bond-layer interface. As for the nanostructured SCL 8YSZ TBCs, there is no obvious change for the phase composition at 1000 °C and 1200 °C. The phase composition of the fractured surface is mainly $Y_{0.15}Zr_{0.85}O_{1.93}$ and c-ZrO_2 phase. This is because that the coating peels off from the inside of the ceramic coating and was destroyed layer by layer, without any spallation at top-coat/bond coat interface. Therefore, this mechanism of damage is more significant than the formation of a thermally grown oxide (TGO) scale at top-coat/bond-coat interface, commonly promoted by high-temperature oxidation of the bond coat surface, i.e. the thickness of the TGO is not high enough to promote TBC spallation. As for the DCL LZ/8YSZ

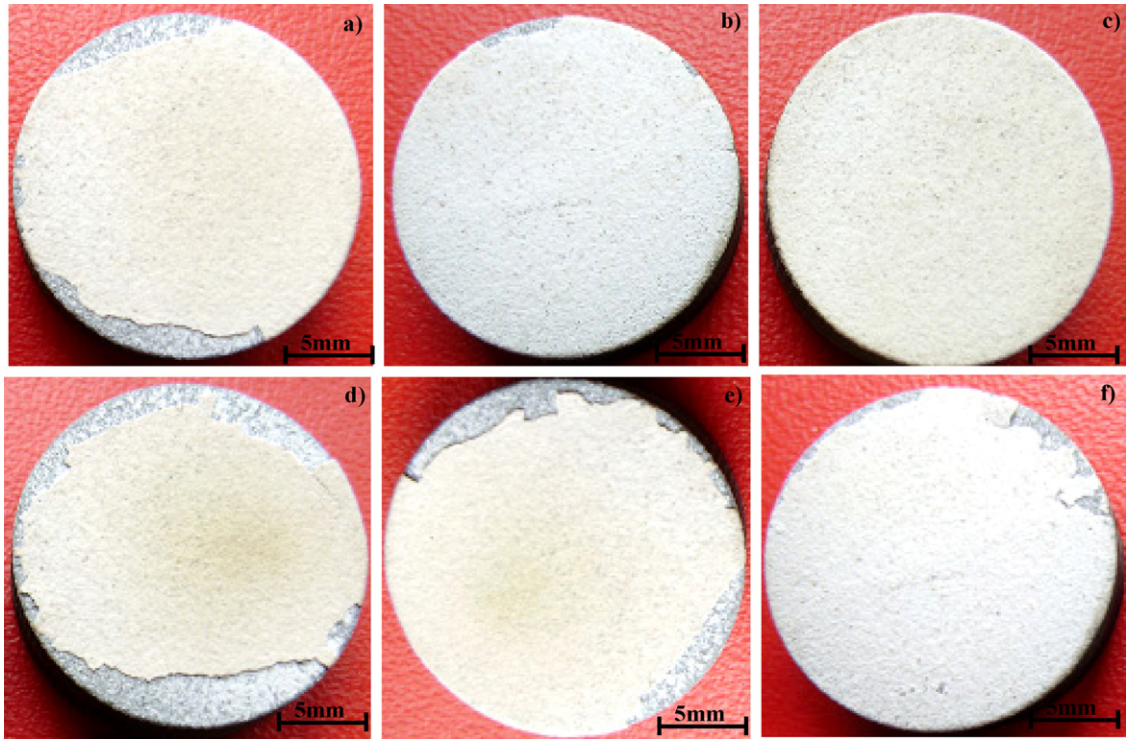

Fig. 5. The macro digital photo of three coatings after thermal shock test at 1000 °C. (a) Conventional SCL 8YSZ after 11 thermal cycles, (b) nanostructured SCL 8YSZ TBCs after 17 thermal cycles, (c) DCL LZ/8YSZ TBCs after 46 thermal cycles, (d) conventional SCL 8YSZ after 53 thermal cycles, (e) nanostructured SCL 8YSZ TBCs after 104 thermal cycles, and (f) DCL LZ/8YSZ TBCs after 158 thermal cycles.

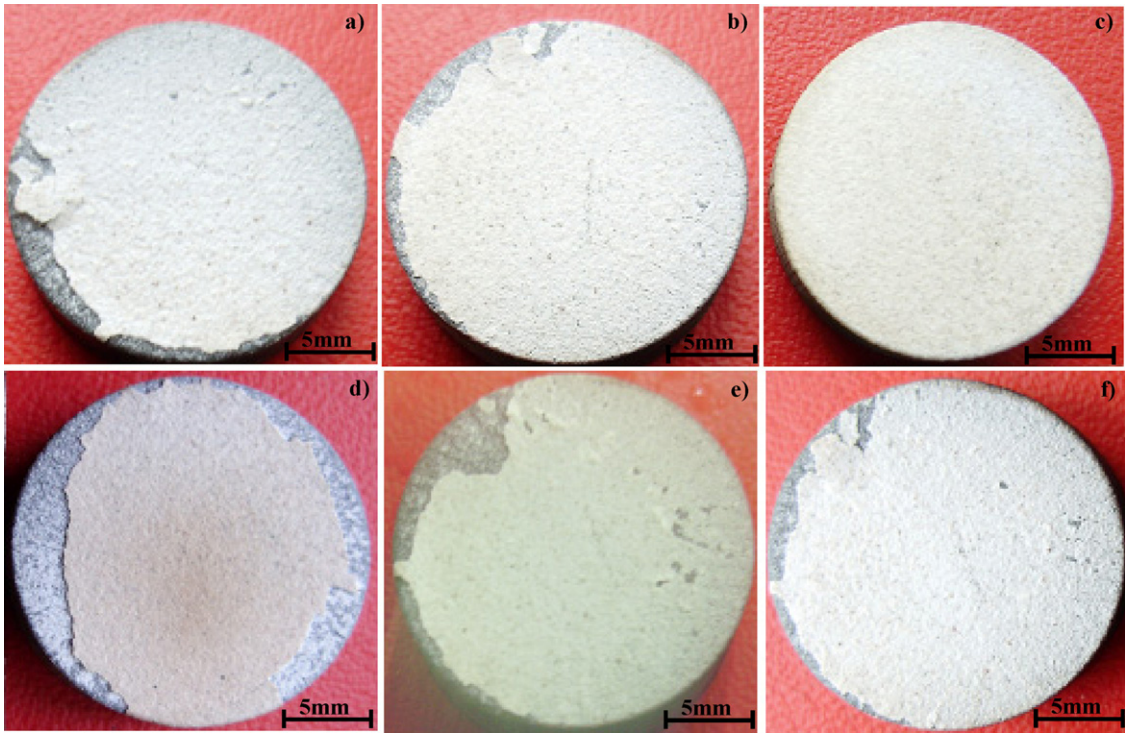

Fig. 6. The macro digital photo of three coatings after thermal shock test at 1200 °C. (a) Conventional SCL 8YSZ after 3 thermal cycles, (b) nanostructured SCL 8YSZ TBCs after 9 thermal cycles, (c) DCL LZ/8YSZ TBCs after 26 thermal cycles, (d) conventional SCL 8YSZ after 7 thermal cycles, (e) nanostructured SCL 8YSZ TBCs after 18 thermal cycles, and (f) DCL LZ/8YSZ TBCs after 43 thermal cycles.

TBCs, the phase composition of the fractured surface at 1000 °C is $La_2Zr_2O_7$, which indicates that the fracture position is at the inner of the upper LZ layer. When the temperature increases to 1200 °C, the phase composition of the fractured surface is $La_2Zr_2O_7$ $Zr_{0.92}Y_{0.08}O_{1.96}$, and t′, which indicate that the fracture occurred at the LZ/8YSZ interface. It can be concluded that the LZ/8YSZ interface will be the weak position at higher temperature.

3.4. Microstrucutre after thermal shock failure at different temperatures

Fig. 8 shows the surface morphology after failure for the three coatings at different thermal shock temperatures. When the temperature is 1000 °C, fine cracks and pores can be seen in the surface of the conventional SCL 8YSZ TBCs after thermal shock failure, and no evident coarse cracks can be seen in the nanostructured 8YSZ TBC. There are more pores in the surface of the DCL LZ/8YSZ TBCs. As LZ has higher sintering resistance ability, many finer pores are retained in the coating. The existence of pores will relieve stress concentration at the tip of the crack and will be beneficial to the improvement of the thermal cycling lifetime. When the temperature is 1200 °C, it can be seen that a big crack run through the coating. This is because the conventional SCL 8YSZ has the lowest sintering resistance ability. When it was exposed to the higher temperature, the sintering phenomenon will be more serious and the pore content of this coating will decrease. At the same time, the thermal expansion coefficient will decrease. The thermal mismatch between the ceramic layer and the metallic layer or the substrate will further increase, so the thermal stress will also increase, bigger cracks can be induced. As for the nanostructured 8YSZ coating, the branched cracks can be observed after failure at 1200 °C, more pores can be observed in this coating compared with the conventional 8YSZ coating. As for the DCL LZ/8YSZ TBCs, finer branched cracks can be seen, many micro-pores distributed at random can be also seen in this coating. The amount of micro-pores will relieve the stress concentration at the crack tip, and the path of the crack propagation can be hampered by the micro-pores and the crack can stop at the position of the pore even be absorbed by the pore. On the other side, the LZ has higher sintering resistance ability compared with the conventional and nanostructured SCL TBCs, and the thermal stress is lower in this coating compared with the nanostructured SCL 8YSZ TBCs which has been investigated in our previous work [33]. In addition, the LZ has lower thermal conductivity compared with the nanostructured 8YSZ and conventional 8YSZ. The LZ layer has a thermal protection effect to the underlying 8YSZ. Lower temperature will be endured for the nanostructured 8YSZ in the DCL LZ/8YSZ TBC compared with the SCL nanostructured TBC. Lower temperature gradient will be produced along the spray direction in the DCL LZ/8YSZ TBC compared with the SCL nanostructured 8YSZ TBC and conventional TBC, and the existence of the LZ layer can inhibit the abnormal growth of the nanostructured 8YSZ grain in the DCL LZ/8YSZ TBCs when the coating are coated on all the sides of the substrates in the actual application, because the crystal grain will grow more

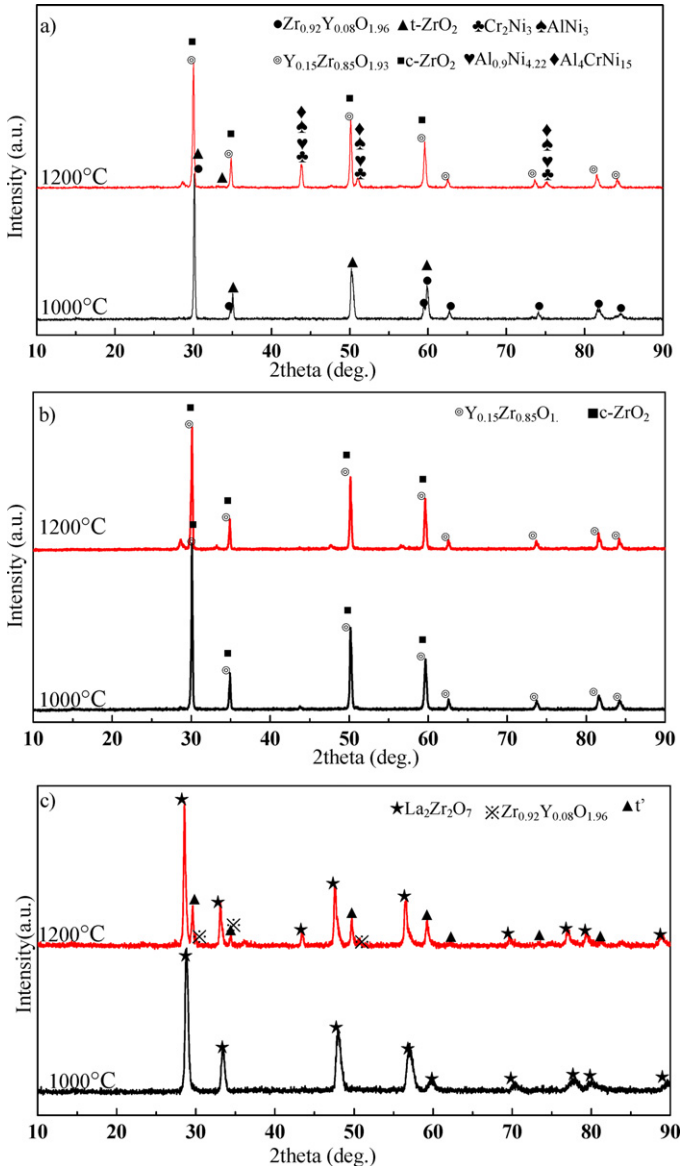

Fig. 7. XRD patterns of the three coatings after thermal shock failure. (a) Conventional SCL 8YSZ TBCs, (b) nanostructured SCL 8YSZ TBCs, and (c) DCL LZ/8YSZ TBCs.

slowly at lower temperature when the initial grain size, heating rate, cooling rate and holding time are the same [34,35]. All of the above aspects will promote the increase of the thermal cycling lifetime of the DCL LZ/8YSZ TBCs.

Fig. 9 shows the fracture surface morphology of the three coatings at different thermal shock temperatures. When the temperature is 1000 °C, the fracture surface of the conventional 8YSZ has exhibited lamellar structural characteristic, and some columnar grains can be seen in the splats. The splats are not tightly connected. Pores and cracks can be seen in the splats and at the interface among the splats. The fracture surfaces of the nanostructured 8YSZ TBCs and the DCL LZ/8YSZ TBCs have not exhibited evident lamellar structural characteristic which is attributed to the reason that their sprayed feedstock has exhibited global morphology and excellent flowability. Some equiaxed grains can be seen in the two coatings. At the same time, pores and cracks are also inevitable in the two coatings. When the temperature increases to 1200 °C, as for the conventional 8YSZ coating, the brittle fracture has occurred at the interface among the splats. The crack propagates along the interface, and the drawing phenomenon occurred in the splats can be also seen in this coating. The vertical crack can be seen and the perfoliate crack which results from the vertical crack can also be observed in this coating. As for the DCL LZ/8YSZ TBCs, the finer branched cracks can be seen in the fracture surface and no evident direction can be observed for this type of crack due to the stress decrease in the DCL LZ/8YSZ TBCs.

Fig. 10 shows the section image before and after thermal shock failure for the three coatings at different temperatures. There are inherent defects inside the coating before the thermal shock, the interface of the coating is nearly keep perfect, no evident crack can be seen at the interface. When the temperature is 1000 °C, there are big vertical cracks and perfoliate horizontal cracks which propagate along the ceramic layer/bond-layer interface for the conventional 8YSZ TBCs. Some tiny peeling off phenomenon can be observed in the nanostructured 8YSZ and DCL LZ/8YSZ TBCs at 1000 °C. Pores distributed at random inside the ceramic coating can also be seen, and the existed pores can scatter and relieve the stress concentration during the thermal shock and will help to improve the thermal cycling lifetime of the coatings. When the thermal shock temperature increases to 1200 °C, the evident cracking phenomenon can be seen due to the propagation of the vertical crack and the propagation of the horizontal crack along the interface for the conventional 8YSZ coating. There are also some small vertical cracks and horizontal cracks in the nanostructured 8YSZ. But as for the DCL LZ/8YSZ TBCs, only some fine cracks propagated from the surface into the interface between 8YSZ layer and the bond coat. To sum up, the nanostructured 8YSZ coatings exhibit higher thermal shock resistance ability than that of the conventional 8YSZ coatings, this enhancement can be explained in terms of higher resistance to crack propagation [36]. Indeed, the presence of porous nanosized areas which came from the un-molten feedstock particles and being retained in the coating increase the compliance and counteract the sintering effects, thus partially preventing the densification of the porous microstructure. In view of this, nanostructured plasma sprayed YSZ coatings are very promising for TBC applications, due to their relatively low degree of degradation, lower residual tensile stress in plane [37] and higher thermal cycling lifetime. In addition, the nanostructured TBC has higher creep rate compared with the conventional TBC at high temperature, this indicated that more rapid stress relaxation and degraded tensile stresses upon cooling and yielding to cracking and spallation in the nanostructured TBC. The high toughness and the low Young's modulus (low tensile residual stress in plane) of the nanostructured 8YSZ coating make sure that it has improved thermal cycling lifetime [38]. As for the DCL LZ/8YSZ, firstly, the phase stability of the LZ layer is very good. There is no decomposition or phase destabilization for the LZ layer at the present thermal shock temperatures. And it is worth noting that

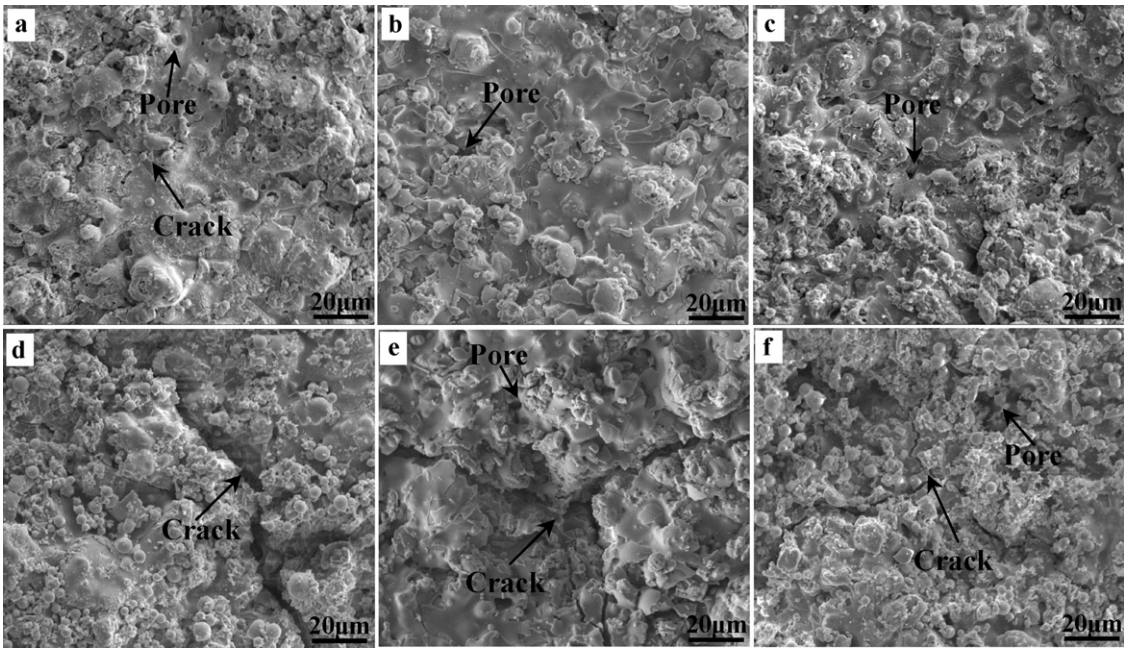

Fig. 8. Surface morphology of the three coatings after failure. Conventional SCL 8YSZ (a), nanostructured SCL 8YSZ (b) and DCL LZ/8YSZ TBCs (c) at 1000 °C after failure; conventional SCL 8YSZ (d) nanostructured SCL 8YSZ (e) and DCL LZ/8YSZ TBCs (f) at 1200 °C after failure.

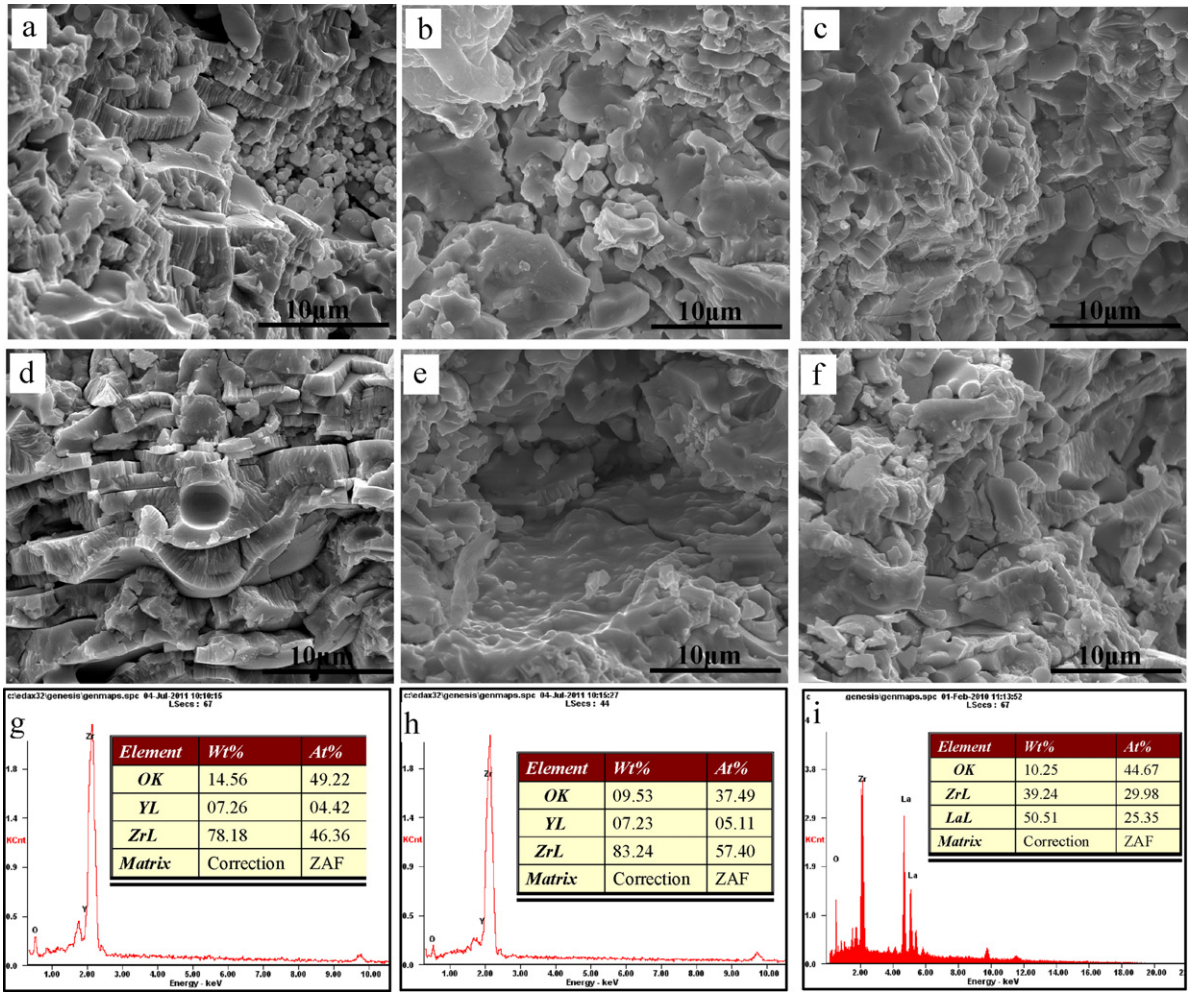

Fig. 9. The fracture surface morphology of the three coatings. (a), (b) and (c) are conventional 8YSZ, nanostructured 8YSZ and DCL LZ/8YSZ respectively at 1000 °C; (d), (e) and (f) are conventional 8YSZ, nanostructured 8YSZ and DCL LZ/8YSZ respectively at 1200 °C; (g), (h) and (i) are corresponding EDS result of the three coatings.

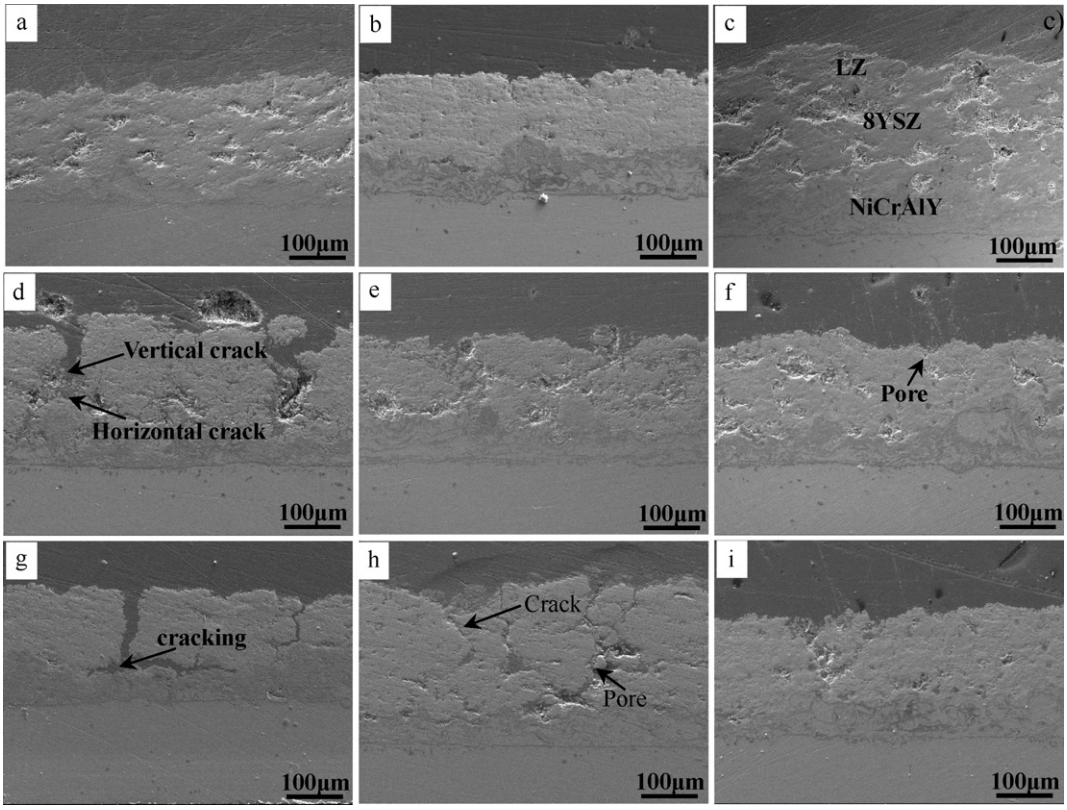

Fig. 10. The section image before and after thermal shock. (a), (b) and (c) are section image of the as-sprayed conventional 8YSZ, nanostructured 8YSZ and DCL LZ/8YSZ TBCs, respectively; (d), (e) and (f) are the section image of the conventional 8YSZ, nanostructured 8YSZ and DCL LZ/8YSZ TBCs after thermal shock failure at 1000 °C, respectively; (g), (h) and (i) are the section image of the conventional 8YSZ, nanostructured 8YSZ and DCL LZ/8YSZ TBCs after thermal shock failure at 1200 °C, respectively.

the actual surface temperature is lower than the thermal shock temperature which is being set by us. Although the LZ layer will also sinter during thermal cycling process, but the sintering resistance ability of the LZ layer is superior to that of the 8YSZ layer. As we know, the elastic modulus will increase with the exposure time increasing at high temperature, which will increase the thermal mismatch and the residual stress between the coating and the substrate. At the same time, the LZ Layer has a thermal protection effect to the underlying 8YSZ layer. The temperature of the YSZ layer is reduced. All of the above factors make that the DCL LZ/8YSZ TBCs have improved thermal shock resistance ability compared with the SCL 8YSZ TBC.

3.5. Mechanism of thermal shock failure

Fig. 11 shows the illustration of surface stress state of the TBCs during heating–cooling cycles and the evolution of coating damage at 1200 °C and 1000 °C. When the temperature is 1200 °C, the conventional SCL 8YSZ TBCs has exhibited laminar structure, amounts of splats are intertwined and arranged to form the ceramic coating. Cracks can be easily induced at the interface among the splats which is attributed to the produce of the thermal residual stress during plasma spraying [39–42]. The crack tends to propagate along the spray direction due to the tensile radial stress with high magnitude, and reach to the interface between the ceramic layer and the metallic layer. The horizontal crack can be formed at the interface and propagate along the interface [43–45]. Subsequently, the interface cracking phenomenon can be observed. As for the nanostructured SCL TBC, it has not exhibited evident laminar structural characteristic due to the characteristic of the nanostructured sprayable feedstock. The produce of the cracks are attributed to the brittles of the ceramic coating resulting from the thermal stress during thermal spraying and thermal shock [46,47]. Crack also tends to propagate along the spray direction. As there are not splats, the splat interface did not exist, the cracks will go through the crack or pores and reach to the metallic-layer/ceramic-layer interface, and eventually cracking along the interface occurred under the action of tensile radial stress at the interface. As for the DCL LZ/8YSZ TBCS, there existed lower tensile radial stress on the surface. More energy will be consumed when a pre-existing surface crack began to propagate, and the thermal protection of LZ layer to the underlying 8YSZ layer due to lower thermal conductivity compared with the 8YSZ. Even a crack has propagated, it will consume much energy when it is nearly to reach the LZ/8YSZ interface. The propagation will stop at the position near the LZ/8YSZ interface. That is why the DCL LZ/8YSZ TBCs have the improved thermal shock resistance ability compared with the conventional and nanostructured SCL 8YSZ TBCs. When the temperature decrease to 1000 °C, the pores

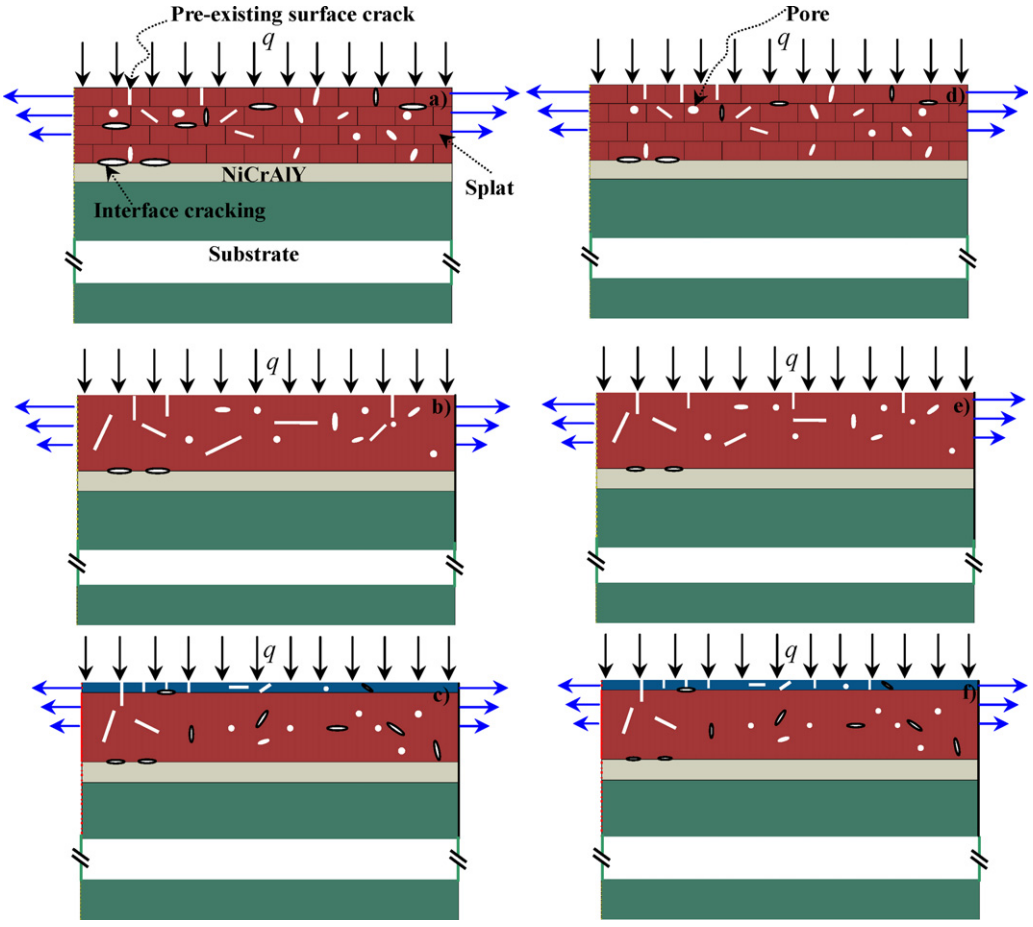

Fig. 11. Stress illustration of the coating surface stress state during heating–cooling cycles and the evolution of coating damage at 1200 °C and 1000 °C thermal cycle. (a) Conventional SCL 8YSZ, (b) nanostructured SCL 8YSZ, (c) DCL LZ/8YSZ TBCs at 1200 °C thermal cycle. (d) Conventional SCL 8YSZ, (e) nanostructured SCL 8YSZ, (f) DCL LZ/8YSZ TBCs at 1000 °C thermal cycle.

and cracks in all the three coatings tend to be finer, as there existed lower temperature gradient and lower thermal stress during the thermal shock. The driving force which can promote the crack to propagate is becoming smaller, the thermal cycling lifetime will increase compared with the case at 1200 °C.

Fig. 12 shows the crack propagation patterns in TBCs during thermal shock. It can be seen that there are three patterns for the propagation of the crack. For the first pattern, when a pre-existed surface crack has been impeded by a crack during the thermal shock, if it has enough energy (such as high temperature gradient), it may go through the crack and continue to propagate and at last reach to the metallic-layer/ceramic-layer interface [48,49], and a horizontal crack along the interface will be formed. For the second case, when a pre-existed surface crack has been impeded by a pore during the thermal shock, if it has enough energy (such as high temperature gradient), it may go through the pore and continue to propagate and at last reach to the metallic-layer/ceramic-layer interface, and a horizontal crack along the interface will also be formed. But when the crack has not enough energy (such as low temperature gradient or low activation energy of crack propagation), it may stop propagation and cannot reach to the interface, this is just the third case. On the other hand, the pre-existed pores will release the stress concentration and decrease the overall stress level and may eventually delay the propagation rate of the main crack. In addition, some finer cracks can be healed and the sintering neck will be formed during the high temperature duration, and further increase the

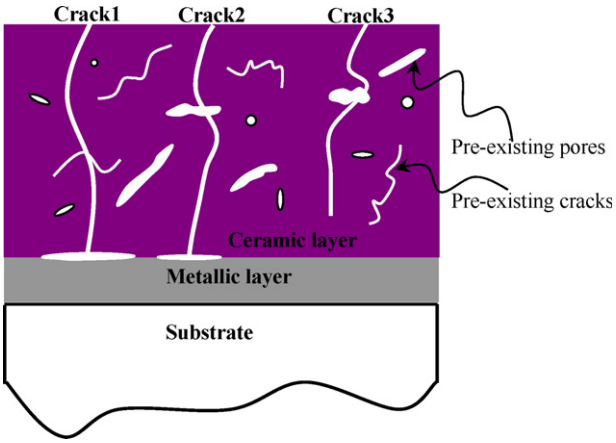

Fig. 12. Schematic illustration of the crack propagating model in TBCs during thermal shock.

stress intensity of the main crack and promote the propagation of the main crack [50–52].

The thickness of the coating also has a very strong impact on the thermal shock behavior of the as-sprayed coating. Indeed, the thick TBC will be beneficial to the improvement of the thermal insulation effect, but higher stress will be produced in the thick TBC which make the thermal cycling lifetime decline when it was exposed to high temperature environment. When the thickness of the coating is high, it can bring to the following effects: Firstly, greater thermal gradient will be caused in the thick TBC during the thermal shock across the whole coating thickness and consequently higher thermal stresses will be produced within the whole coating system. Secondly, both the elastic strain energy stored and the energy release rate for a crack will also increase. These two factors will promote the failure of the thick coatings. On the other aspects, more vertical cracks will be produced when the thickness of the coating is high due to the higher tensile stress in plane. The existence of the vertical cracks can improve the strain tolerance of the TBC significantly which relaxes the thermal stresses greatly. Consequently, the time needed to develop a main crack of sufficient size that initiates buckling or delaminating will increase. Only the vertical crack consume enough energy (thermally activated time is long enough) and propagate to the interface, then the nucleation and growth of horizontal cracks along the interface eventually lead to coating delamination and loss of thermal protection for the system.

4. Conclusions

In this paper, DCL LZ/8YSZ TBCs, nanostructured SCL 8YSZ TBCs and conventional SCL 8YSZ TBCs were fabricated by atmospheric plasma spraying. The microstructure, phase composition and thermal shock behavior of these three coatings were investigated systematically. Some important and useful results can be obtained from the present studies:

(1) The DCL LZ/8YSZ TBCs has better thermal shock resistance ability compared with the nanostructured and conventional SCL 8YSZ TBCs at 1200 °C and 1000 °C which is attributed to the decline of the stress level in the DCL LZ/8YSZ and the thermal protection of LZ layer to the underlying nanostructured 8YSZ layer. And the nanostructured SCL 8YSZ TBCs has improved thermal shock resistance ability compared with the conventional SCL 8YSZ TBCs due to the lower tensile radial stress in plane and the higher fracture toughness.
(2) The thermal cycling lifetimes are correlated with the microstructure of the coating and the structural characteristic of the defects in the coating. The failure modes of the as-sprayed coatings at different thermal shock temperatures are determined by the thermal stress with different magnitude and crack propagation path. Pre-existed cracks in the surface propagate toward the interface vertically under the thermal activation, and the horizontal crack nucleation and growth eventually lead to the failure of the coating.
(3) The DCL coating has a longer thermal cycling lifetime than that of the SCL YSZ coating, indicating that DCL structure is an efficient way to use the advantages and overcome the disadvantages of different coating materials, which is promising for its application at higher temperature. Since no single material that has been studied so far satisfies all the requirements of TBCs, the DCL coating may be an important development direction.

Acknowledgments

This work was supported by the program of excellent team at Harbin Institute of Technology. The authors are grateful to Miss Shufen Chen for the assistance in the thermal shock experiment.

References

[1] N.P. Padture, M. Gell, E.H. Jordan, Thermal barrier coatings for gas-turbine engine applications, Science 296 (2002) 279–284.
[2] A.G. Evans, D.R. Mumm, J.W. Hutehinson, G.H. Meier, F.S. Pettit, Mechanisms controlling the durability of thermal barrier coatings, Prog. Mater. Sci. 46 (2001) 505–553.
[3] A.G. Evans, M.Y. He, J.W. Hutchinson, Mechanics-based scaling laws for the durability of thermal barrier coatings, Prog. Mater. Sci. 2001 (46) (2001) 249–271.
[4] S.C. Joshi, H.W. Ng, Optimizing functionally graded nickel-zirconia coating profiles for thermal stress relaxation, Simul. Model. Pract. Theory 19 (2011) 586–598.
[5] S. Uwe, L. Christoph, F. Klaus, P. Manfred, S.B. Bilge, L. Odile, Some recent trends in research and technology of advanced thermal barrier coatings, Aerosp. Sci. Technol. 7 (2003) 73–80.
[6] P. Ramaswamy, S. Seetharamu, K.B.R. Varma, K.J. Rao, Evaluation of $CaO–CeO_2$ partially stabilized zirconia thermal barrier coatings, Ceram. Int. 25 (1999) 317–324.
[7] S. Das, S. Datta, D. Basu, G.C. Das, Glass-ceramics as oxidation resistant bond coat in thermal barrier coating system, Ceram. Int. 35 (2009) 1403–1406.
[8] S.Q. Guo, Y. Kagawa, Effect of thermal exposure on hardness and Young's modulus of EB-PVD yttria-partially-stabilized zirconia thermal barrier coatings, Ceram. Int. 32 (2006) 263–270.
[9] S.Q. Guo, Y. Kagawa, Isothermal and cycle properties of EB-PVD yttria-partially-stabilized zirconia thermal barrier coatings at 1150 and 1300 °C, Ceram. Int. 33 (2007) 373–378.
[10] G.D. Girolamo, C. Blasi, M. Schioppa, L. Tapfer, Structure and thermal properties of heat treated plasma sprayed ceria-yttria co-stabilized zirconia coatings, Ceram. Int. 36 (2010) 961–968.
[11] R.W. Steinbrech, V. Postolenko, J. Mönch, J. Malzbender, L. Singheiser, Testing method to assess lifetime of EB-PVD thermal barrier coatings on tubular specimens in static and cyclic oxidation tests, Ceram. Int. 37 (2011) 363–368.
[12] E.P. Busso, L. Wright, H.E. Evans, L.N. McCartney, S.R.J. Saunders, S. Osgerby, J. Nunn, A physics-based life prediction methodology for thermal barrier coating systems, Acta Mater. 55 (2007) 1491–1503.
[13] D. Cojocaru, A.M. Karlsson, A simple numerical method of cycle jumps for cyclically loaded structures, Int. J. Fatigue 28 (2006) 1677–1689.
[14] D.M. Zhu, S.R. Choi, R.A. Miller, Development and thermal fatigue testing of ceramic thermal barrier coatings, Surf. Coat. Technol. 188 (2004) 146–152.
[15] Y. Li, C.J. Li, Q. Zhang, G.J. Yang, C.X. Li, Influence of TGO composition on the thermal shock lifetime of thermal barrier coatings with cold-sprayed MCrAlY bond coat, J. Therm. Spray Technol. 19 (2010) 168–177.
[16] H.B. Guo, Y. Wang, L. Wang, S.K. Gong, Thermo-physical properties and thermal shock resistance of segmented $La_2Ce_2O_7$/YSZ thermal barrier coatings, J. Therm. Spray Technol. 18 (2009) 665–671.

[17] B. Saeedi, A. Sabour, A.M. Khoddami, Study of microstructure and thermal shock behavior of two types of thermal barrier coatings, Mater. Corros. 60 (2009) 695–703.
[18] F.F. Xu, J.H. Yu, X.L. Mou, L.L. Zhang, S.Y. Tao, Structures and morphology of the ordered domains in $Sm_2Zr_2O_7$ coatings, Chem. Phys. Lett. 492 (2010) 235–240.
[19] Z.H. Xu, L.M. He, R.D. Mu, S.M. He, G.H. Huang, X.Q. Cao, Double-ceramic-layer thermal barrier coatings based on $La_2(Zr_{0.7}Ce_{0.3})_2O_7$/$La_2Ce_2O_7$ deposited by electron beam-physical vapor deposition, Appl. Surf. Sci. 256 (2010) 3661–3668.
[20] R. Vassen, X.Q. Cao, F. Tietz, D. Basu, D. Stöver, Zirconate as new materials for thermal barrier coatings, J. Am. Ceram. Soc. 83 (2000) 2023–2028.
[21] L.M. He, Z.H. Xu, X.Q. Cao, X.H. Zhong, R.D. Mu, S.M. He, Adhesive strength of new thermal barrier coatings of rare earth zirconates, Vacuum 83 (2009) 1388–1392.
[22] R. Vaßen, F. Traeger, D. Stöver, New thermal barrier coatings based on pyrochlore/YSZ double-layer systems, Int. J. Appl. Ceram. Technol. 1 (2004) 351–361.
[23] H.M. Zhou, D.Q. Yi, Z.M. Yu, L.R. Xiao, Preparation and thermophysical properties of CeO_2 doped $La_2Zr_2O_7$ ceramic for thermal barrier coatings, J. Alloys Compd. 438 (2007) 217–221.
[24] X.L. Chen, Y.F. Zhang, X.H. Zhong, Z.H. Xu, J.F. Zhang, Y.L. Cheng, Y. Zhao, Y.J. Liu, X.Z. Fan, Y. Wang, H.M. Ma, X.Q. Cao, Thermal cycling behaviors of the plasma sprayed thermal barrier coatings of hexaluminates with magnetoplumbite structure, J. Eur. Ceram. Soc. 30 (2010) 1649–1657.
[25] H. Dai, X.H. Zhong, J.Y. Li, Y.F. Zhang, J. Meng, X.Q. Cao, Thermal stability of double-ceramic-layer thermal barrier coatings with various coating thickness, Mater. Sci. Eng. A 433 (2006) 1–7.
[26] Z.H. Xu, S.M. He, L.M. He, R.D. Mu, G.H. Huang, X.Q. Cao, Novel thermal barrier coatings based on $La_2(Zr_{0.7}Ce_{0.3})_2O_7$/8YSZ double-ceramic-layer systems deposited by electron beam physical vapor deposition, J. Alloys Compd. 509 (2011) 4273–4283.
[27] Z.H. Xu, L.M. He, R.D. Mu, X.H. Zhong, Y.F. Zhang, J.F. Zhang, X.Q. Cao, Double-ceramic-layer thermal barrier coatings of $La_2Zr_2O_7$/YSZ deposited by electron beam-physical vapor deposition, J. Alloys Compd. 473 (2009) 509–515.
[28] X.Y. Xie, H.B. Guo, S.K. Gong, H.B. Xu, Thermal cycling behavior and failure mechanism of $LaTi_2Al_9O_{19}$/YSZ thermal barrier coatings exposed to gas flame, Surf. Coat. Technol. 205 (2011) 4291–4298.
[29] M.H. Li, X.F. Sun, W.Y. Hu, H.G. Guan, Thermal shock behavior of EB-PVD thermal barrier coatings, Surf. Coat. Technol. 201 (2007) 7387–7391.
[30] Y. Wang, H.B. Guo, S.K. Gong, Thermal shock resistance and mechanical properties of $La_2Ce_2O_7$ thermal barrier coatings with segmented structure, Ceram. Int. 35 (2009) 2639–2644.
[31] L. Wang, Y. Wang, X.G. Sun, J.Q. He, Z.Y. Pan, L.L. Yu, Preparation and characterization of nanostructured $La_2Zr_2O_7$ feedstock used for plasma spraying, Powder Technol. 212 (2011) 267–277.
[32] G.D. Girolamo, C. Blasi, L. Pagnotta, M. Schioppa, Phase evolution and thermophysical properties of plasma sprayed thick zirconia coatings after annealing, Ceram. Int. 36 (2010) 2273–2280.
[33] L. Wang, Y. Wang, X.G. Sun, J.Q. He, Z.Y. Pan, C.H. Wang, Finite element simulation of residual stress of double-ceramic-layer $La_2Zr_2O_7$/8YSZ thermal barrier coatings using birth and death element technique, Comput. Mater. Sci. 53 (2012) 117–127.
[34] N. Wang, C.G. Zhou, S.K. Gong, H.B. Xu, Heat treatment of nanostructured thermal barrier coating, Ceram. Int. 33 (2007) 1075–1081.
[35] L. Wang, Y. Wang, X.G. Sun, J.Q. He, Z.Y. Pan, C.H. Wang, A novel structure design towards extremely low thermal conductivity for thermal barrier coatings: experimental and mathematical study, Mater. Des. 35 (2011) 505–517.
[36] L. Wang, Y. Wang, X.G. Sun, J.Q. He, Z.Y. Pan, C.H. Wang, Microstructure and indentation mechanical properties of plasma sprayed nano-bimodal and conventional ZrO_2–8wt%Y_2O_3 thermal barrier coatings, Vacuum (2011), doi:10.1016/j.vacuum.2011.10.029.
[37] L. Wang, Y. Wang, X.G. Sun, Z.Y. Pan, J.Q. He, Y. Zhou, P.L. Wu, Microstructure and surface residual stress of plasma sprayed nanostructured and conventional ZrO_2–8wt%Y_2O_3 thermal barrier coatings, Surf. Interface Anal. 43 (2011) 869–880.
[38] G.D. Girolamo, F. Marra, C. Blasi, E. Serra, T. Valente, Microstructure, mechanical properties and thermal shock resistance of plasma sprayed nanostructured zirconia coatings, Ceram. Int. 37 (2011) 2711–2717.
[39] H.W. Ng, Z. Gan, A finite element analysis technique for predicting as-sprayed residual stresses generated by the plasma spray coating process, Finite Elem. Anal. Des. 41 (2005) 1235–1254.
[40] H.B. Guo, R. Vaßen, D. Stöver, Atmospheric plasma sprayed thick thermal barrier coatings with high segmentation crack density, Surf. Coat. Technol. 186 (2004) 353–363.
[41] A.N. Khan, J. Lu, Behavior of air plasma sprayed thermal barrier coatings, subject to intense thermal cycling, Surf. Coat. Technol. 166 (2003) 37–43.
[42] A.N. Khan, J. Lu, Thermal cyclic behavior of air plasma sprayed thermal barrier coatings sprayed on stainless steel substrates, Surf. Coat. Technol. 201 (2007) 4653–4658.
[43] B. Zhou, K. Kokini, Effect of pre-existing surface crack morphology on the interfacial thermal fracture of thermal barrier coatings: a numerical study, Mater. Sci. Eng. A 348 (2003) 271–279.
[44] B. Zhou, K. Kokini, Effect of preexisting surface cracks on the interfacial thermal fracture of thermal barrier coatings: an experimental study, Surf. Coat. Technol. 187 (2004) 17–25.
[45] B. Zhou, K. Kokini, Effect of surface pre-crack morphology on the fracture of thermal barrier coatings under thermal shock, Acta Mater. 52 (2004) 4189–4197.
[46] C.G. Zhou, N. Wang, H.B. Xu, Comparison of thermal cycling behavior of plasma-sprayed nanostructured and traditional thermal barrier coatings, Mater. Sci. Eng. A 452 (2007) 569–574.
[47] C.B. Liu, Z.M. Zhang, X.L. Jiang, M. Liu, Z.H. Zhu, Comparison of thermal shock behaviors between plasma-sprayed nanostructured and conventional zirconia thermal barrier coatings, Trans. Nonferrous Met. Soc. China 19 (2009) 99–107.
[48] A. Gilbert, K. Kokini, S. Sankarasubramanian, Thermal fracture of zirconia–mullite composite thermal barrier coatings under thermal shock: an experimental study, Surf. Coat. Technol. 202 (2008) 2152–2161.
[49] A. Gilbert, K. Kokini, S. Sankarasubramanian, Thermal fracture of zirconia–mullite composite thermal barrier coatings under thermal shock: a numerical study, Surf. Coat. Technol. 203 (2008) 91–98.
[50] Q.H. Yu, A. Rauf, N. Wang, C.G. Zhou, Thermal properties of plasma-sprayed thermal barrier coating with bimodal structure, Ceram. Int. 37 (2011) 1093–1099.
[51] B. Siebert, R. Vassen, D. Stover, Changes in porosity and Young's modulus due to sintering of plasma sprayed thermal barrier coatings, J. Mater. Process. Technol. 92-93 (1999) 217–223.
[52] V. Lughi, V.K. Tolpygo, D.R. Clarke, Microstructural aspects of the sintering of thermal barrier coatings, Mater. Sci. Eng. A 368 (2004) 212–221.